Energy losses of charged particles moving parallel to the surface of an overlayer system

C. M. Kwei, S. J. Hwang, Y. C. Li, and C. J. Tung

Citation: Journal of Applied Physics **93**, 9130 (2003); doi: 10.1063/1.1569974
View online: http://dx.doi.org/10.1063/1.1569974
View Table of Contents: http://scitation.aip.org/content/aip/journal/jap/93/11?ver=pdfcov
Published by the AIP Publishing

Energy losses of charged particles moving parallel to the surface of an overlayer system

C. M. Kwei,[a] S. J. Hwang, and Y. C. Li
Department of Electronics Engineering, National Chiao Tung University, Hsinchu 300, Taiwan

C. J. Tung
Department of Nuclear Science, National Tsing Hua University, Hsinchu 300, Taiwan

(Received 22 November 2002; accepted 6 March 2003)

An energetic charged particle moving parallel to the surface of an overlayer system was studied. This system was composed of a thin film on the top of a semi-infinite substrate. Based on the dielectric response theory, the induced potential was formulated by solving the Poisson equation and matching the boundary conditions. The stopping force was built-up using the energy-momentum conservation relations and the extended Drude dielectric functions with spatial dispersion. Surface (vacuum–film) and interface (film–substrate) excitations were included in the formulations of the interaction between charged particles and the overlayer system. Results of the wake potential were presented for protons moving parallel to a vacuum–copper–silicon system. Dependences of the induced potential and the stopping force on film thickness, distance of the proton from surface, and proton velocity were investigated. © *2003 American Institute of Physics.*
[DOI: 10.1063/1.1569974]

I. INTRODUCTION

Many experimental and theoretical studies have been performed on the various aspects of the interaction between fast charged particles and solid surfaces. Theoretical approaches[1–3] were developed for the evaluation of the induced potential caused by charged particles traveling outside a solid and parallel to its surface. This potential arose from the dielectric response of the solid and led to, mainly, surface plasmon excitations. Theoretical calculations of surface excitations were made in earlier works.[4,5] The surface response was characterized in terms of the dielectric function of the bulk material. Several models and approximations of the dielectric function[6–8] were developed.

A study of the induced potential in an overlayer system (film on substrate) is important when dealing with the production of electrons by swift ions and with the transport of convoy electrons on their emission[9,10] and acceleration.[11,12] In such a study, it is required to provide data on the induced potential and the stopping force for charged particles. Thus certain procedures have to be established in order to make accurate predictions of these quantities. The purpose of this work was to derive a model treatment of the induced potential for charged particles moving outside an overlayer system and parallel to its surface (vacuum–solid) and interface (film–substrate). The interaction of charged particles with the overlayer system includes not only surface excitations but also interface excitations. Models developed for the semi-infinite solids should not be applied directly to the overlayer system.

Previously, a model[13,14] of the energy loss probability was constructed for an overlayer system by several authors. Integration over the normal component of the momentum transfer was carried out using cylindrical coordinates. This model, however, did not completely satisfy the conservation constraints in energy and momentum. In order to satisfy these constraints, we applied in this work spherical coordinates in the momentum integration. Moreover, the induced potential was derived by solving the Poisson equation using methods of image charges and extended Drude dielectric functions with spatial dispersion.[15] The image charge was external to the region of interest and used to simulate the required boundary conditions. The inclusion of dispersion was important in the region of short distances from the surface and the interface, where charged particles might couple to short-wavelength modes of the overlayer system.[1] The dielectric function used in this work was a generalization of the Drude dielectric function by allowing each subband to have its own oscillator strength, damping constant, and critical point energy. All parameters in the dielectric function were properly chosen to fit optical data and to meet sum-rule requirements. This function was successfully employed to describe the response of a semi-infinite solid and an overlayer system for penetrating electrons.[16–21]

In this work, we have calculated the induced potential and the electric field for protons moving parallel to the surface of an overlayer system composed of a thin Cu film on the top of a semi-infinite Si substrate. Since surface excitations involved electrons within a few angstroms beneath the surface, we considered here films of a few angstrom thickness in the overlayer system to illustrate its surface and interface effects. Atomic units (a.u.) are used throughout this article unless otherwise specified.

II. THEORY

Figure 1 illustrates the problem studied in this work, i.e., a particle of charge q and velocity $\mathbf{v}$ moving parallel to the

[a]Electronic mail: cmkwei@mail.nctu.edu.tw

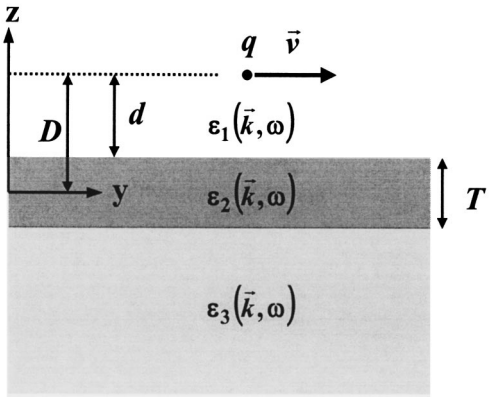

FIG. 1. A sketch of the problem studied in this work. A particle with charge q and velocity v, in y direction, moving in vacuum (medium 1) and parallel to the surface of an overlayer system. This system is composed of a film (medium 2) of thickness T on top of a substrate (medium 3). The particle is at distance D from the midplane of the film, or at distance d from the surface of the film. ε_1, ε_2, and ε_3 are, respectively, dielectric functions of media 1, 2, and 3.

surface of an overlayer system composed of a thin film on the top of a semi-infinite substrate. To simplify theoretical derivations, we let the origin of coordinates be the center of the film having thickness T and dielectric function $\varepsilon_2(\mathbf{k},\omega)$. The vacuum and substrate, characterized by their dielectric functions $\varepsilon_1(\mathbf{k},\omega)$ and $\varepsilon_3(\mathbf{k},w)$, are in regions of $z>T/2$ and $z<-T/2$, where the z axis is perpendicular to the interface planes and directed from substrate to film. The particle, with a z coordinate equal to D, is moving in the vacuum along the y direction.

For $z>T/2$, the potential is due to the actual charge and a fictitious charge near the surface just outside the region of interest. For $z<T/2$, the potential is a solution of the Laplace equation without singularities since there is no charge there. In the latter region, the simplest assumption is that the potential is contributed by an image charge q at the position of the actual charge and by fictitious charges near the interfaces. These fictitious charges should satisfy the required boundary conditions. Thus Poisson equations in the Fourier space are

$$\phi_1(\mathbf{k},\omega)=\frac{4\pi}{k^2\varepsilon_1(\mathbf{k},\omega)}\left[\rho_f(\mathbf{k},\omega)+\exp\left(-\frac{ik_zT}{2}\right)\rho_{s1}(\mathbf{K},\omega)\right] \tag{1}$$

for $z>T/2$,

$$\phi_2(\mathbf{k},\omega)=\frac{4\pi}{k^2\varepsilon_2(\mathbf{k},\omega)}\left[\rho_f(\mathbf{k},\omega)+\exp\left(-\frac{ik_zT}{2}\right)\rho_{s2}^{+}(\mathbf{K},\omega)+\exp\left(\frac{ik_zT}{2}\right)\rho_{s2}^{-}(\mathbf{K},\omega)\right] \tag{2}$$

for $-T/2<z<T/2$, and

$$\phi_3(\mathbf{k},\omega)=\frac{4\pi}{k^2\varepsilon_3(\mathbf{k},\omega)}\left[\rho_f(\mathbf{k},\omega)+\exp\left(\frac{ik_zT}{2}\right)\rho_{s3}(\mathbf{k},\omega)\right] \tag{3}$$

for $z<-T/2$, where $\mathbf{k}=(k_x,k_y,k_z)=(\mathbf{K},k_z)$ is the momentum transfer, ω is the energy transfer, and the Fourier transform of the charge density distribution of the moving particle is given by

$$\rho_f(\mathbf{k},\omega)=2\pi q\,\delta(\omega-k_yv)\exp(-ik_zD). \tag{4}$$

The induced charges $\rho_{s1}(\mathbf{K},\omega)$, $\rho_{s2}^{+}(\mathbf{K},\omega)$, $\rho_{s2}^{-}(\mathbf{K},\omega)$, and $\rho_{s3}(\mathbf{K},\omega)$ are required to satisfy the boundary conditions. By matching potentials and displacement vectors at the interfaces, we have

$$\rho_{s1}(\mathbf{K},\omega)=2\pi q\,\delta(\omega-k_yv)\left\{\frac{\eta_{12}(T/2,D,\mathbf{K},\omega)[e^{-KT}-\xi_{32}(-T/2,\mathbf{K},\omega)]-\eta_{32}(-T/2,D,\mathbf{K},\omega)[1-e^{-KT}\xi_{12}(T/2,\mathbf{K},\omega)]}{\xi_{12}(T/2,\mathbf{K},\omega)\xi_{32}(-T/2,\mathbf{K},\omega)-1}\right\}, \tag{5}$$

$$\rho_{s2}^{+}(\mathbf{K},\omega)=2\pi q\,\delta(\omega-k_yv)\left[\frac{\eta_{12}(T/2,D,\mathbf{K},\omega)\xi_{32}(-T/2,\mathbf{K},\omega)-\eta_{32}(-T/2,D,\mathbf{K},\omega)}{\xi_{12}(T/2,\mathbf{K},\omega)\xi_{32}(-T/2,\mathbf{K},\omega)-1}\right], \tag{6}$$

$$\rho_{s2}^{-}(\mathbf{K},\omega)=2\pi q\,\delta(\omega-k_yv)\left\{\frac{\eta_{12}(T/2,D,\mathbf{K},\omega)-\eta_{32}(-T/2,D,\mathbf{K},\omega)\xi_{12}(T/2,\mathbf{K},\omega)}{\xi_{12}(T/2,\mathbf{K},\omega)\xi_{32}(-T/2,\mathbf{K},\omega)-1}\right\}, \tag{7}$$

and

$$\rho_{s3}(\mathbf{K},\omega)=2\pi q\,\delta(\omega-k_yv)\left\{\frac{\eta_{32}(-T/2,D,\mathbf{K},\omega)[e^{-KT}-\xi_{12}(T/2,\mathbf{K},\omega)]-\eta_{12}(T/2,D,\mathbf{K},\omega)[1-e^{-KT}\xi_{32}(-T/2,\mathbf{K},\omega)]}{\xi_{12}(T/2,\mathbf{K},\omega)\xi_{32}(-T/2,\mathbf{K},\omega)-1}\right\}, \tag{8}$$

where

$$\eta_{ab}(\pm T/2,D,\mathbf{K},\omega) = \frac{\dfrac{1}{\overline{\overline{\varepsilon_a}}(\pm T/2,-D,\mathbf{K},\omega)} - \dfrac{1}{\overline{\overline{\varepsilon_b}}(\pm T/2,-D,\mathbf{K},\omega)}}{e^{-QT}\dfrac{1}{\overline{\overline{\varepsilon_a}}(\mathbf{K},\omega)} - \dfrac{1}{\overline{\overline{\varepsilon_b}}(\pm T,\mathbf{K},\omega)}}, \tag{9}$$

$$\xi_{ab}(\pm T/2,\mathbf{K},\omega) = \frac{\dfrac{1}{\overline{\overline{\varepsilon_a}}(\mathbf{K},\omega)} + \dfrac{1}{\overline{\overline{\varepsilon_b}}(\mathbf{K},\omega)}}{e^{-QT}\dfrac{1}{\overline{\overline{\varepsilon_a}}(\mathbf{K},\omega)} - \dfrac{1}{\overline{\overline{\varepsilon_b}}(\pm T,\mathbf{K},\omega)}}, \tag{10}$$

$$\frac{1}{\overline{\overline{\varepsilon_L}}(\mathbf{K},\omega)} = \int_{-\infty}^{\infty}\frac{dk_z}{k^2}\left(\frac{1}{\varepsilon_L(\mathbf{k},\omega)}\right), \tag{11}$$

and

$$\frac{1}{\overline{\overline{\varepsilon_L}}(l,\mathbf{K},\omega)} = \int_{-\infty}^{\infty}\frac{dk_z}{k^2}\left(\frac{1}{\varepsilon_L(\mathbf{k},\omega)}\right)\exp(ik_z l) \tag{12}$$

for $a=1$ and 3, $b=2$, and $L=1$, 2, and 3. Substituting Eqs. (5)–(12) into Eqs. (1)–(3), we obtain the scalar potentials in the Fourier space, i.e., $\phi_1(\mathbf{k},\omega)$, $\phi_2(\mathbf{k},\omega)$, and $\phi_3(\mathbf{k},\omega)$. The induced scalar potentials in the spatial space are then obtained by the inverse Fourier transforms after removing the vacuum potential of the particle from the scalar potentials. The induced potential $\phi_{\mathrm{ind}}^{(1)}(\mathbf{r},t)$ for $z>T/2$ is of special interest since the particle is moving in vacuum. Taking $\varepsilon_1=1$, we obtain

$$\phi_{\mathrm{ind}}^{(1)}(\mathbf{r},t) = \int_{-\infty}^{\infty}\frac{d\omega}{2\pi}\int_{-\infty}^{\infty}\frac{d^3k}{(2\pi)^3}\frac{4\pi}{k^2} \times\left[\exp\left(-\frac{ik_zT}{2}\right)\rho_{s1}(\mathbf{K},\omega)\right]\exp[i(\mathbf{k}\cdot\mathbf{r}-\omega t)]. \tag{13}$$

Because of the weak dependence of ε on k_z as compared to the rest of k components in the integral, one may assume $\varepsilon(\mathbf{k},\omega)=\varepsilon(\mathbf{K},\omega)$. The same assumption was adopted by Yubero *et al.*[22,23] in the analysis of reflection-electron energy loss spectra and Kwei *et al.*[20] in the calculation of electron elastic backscattering spectra. Using this assumption, the induced potential in vacuum is obtained by performing the integration over momentum transfer in Eq. (13) with spherical coordinates as

$$\begin{aligned}\phi_{\mathrm{ind}}^{(1)}(\mathbf{r},t) = \frac{q}{2\pi^2}\int_{-\infty}^{\infty}d\omega\int_0^{\infty}dk\int_0^{\pi}d\theta\int_0^{2\pi}d\phi\cdot\sin\theta \\ \cdot\delta(\omega-kv\sin\theta\sin\phi)\zeta(T,d,K,\omega) \\ \times\exp\{i[xk\sin\theta\cos\phi+(y-vt)k \\ \times\sin\theta\sin\phi+(z-T/2)k\cos\theta]\},\end{aligned} \tag{14}$$

where $\mathbf{r}=(x,y,z)$, $d=D-T/2$, and

$$\zeta(T,d,K,\omega) = e^{-dK}\left\{\frac{\dfrac{\varepsilon_2(K,\omega)-1}{\varepsilon_2(K,\omega)+1}\left[1-\dfrac{\varepsilon_3(K,\omega)-\varepsilon_2(K,\omega)}{\varepsilon_3(K,\omega)+\varepsilon_2(K,\omega)}e^{-2TK}\right]}{1+\dfrac{\varepsilon_3(K,\omega)-\varepsilon_2(K,\omega)}{\varepsilon_3(K,\omega)+\varepsilon_2(K,\omega)}\dfrac{\varepsilon_2(K,\omega)-1}{\varepsilon_2(K,\omega)+1}e^{-2TK}} + \frac{\dfrac{\varepsilon_3(K,\omega)-\varepsilon_2(K,\omega)}{\varepsilon_3(K,\omega)+\varepsilon_2(K,\omega)}\left[e^{-TK}+\dfrac{\varepsilon_2(K,\omega)-1}{\varepsilon_2(K,\omega)+1}e^{-3TK}\right]}{1+\dfrac{\varepsilon_3(K,\omega)-\varepsilon_2(K,\omega)}{\varepsilon_3(K,\omega)+\varepsilon_2(K,\omega)}\dfrac{\varepsilon_2(K,\omega)-1}{\varepsilon_2(K,\omega)+1}e^{-2TK}}\right\}. \tag{15}$$

In the above derivations, we have adopted $\varepsilon(\mathbf{K},\omega)=\varepsilon(K,\omega)$.

We now expand the δ function in Eq. (17) as follows:

$$\begin{aligned}\delta(\omega-kv\sin\theta\sin\phi) = \frac{1}{\sqrt{(kv\sin\theta)^2-\omega^2}} \\ \times\left\{\delta\left(\phi-\sin^{-1}\frac{\omega}{kv\sin\theta}\right)\right. \\ \left.+\delta\left[\phi-\left(\pi-\sin^{-1}\frac{\omega}{kv\sin\theta}\right)\right]\right\}\end{aligned} \tag{16}$$

for $\sin^{-1}(\omega/kv)<\theta<[\pi-\sin^{-1}(\omega/kv)]$. After integrating over ϕ in Eq. (17) and applying $\varepsilon(K,-\omega)=\varepsilon^*(K,\omega)$, this equation becomes

$$\begin{aligned}\phi_{\mathrm{ind}}^{(1)}(\mathbf{r},t) = \frac{4q}{\pi^2}\int_0^{\infty}d\omega\int_0^{\infty}dk \\ \times\int_{\sin^{-1}(\omega/kv)}^{\pi/2}d\theta\frac{\sin\theta\cos[k(z-T/2)\cos\theta]}{\sqrt{(k\sin\theta)^2-\omega^2}} \\ \times\cos\left(x\frac{\sqrt{(kv\sin\theta)^2-\omega^2}}{v}\right) \\ \times\left\{\mathrm{Re}[\zeta(T,d,K,\omega)]\cos\left[(y-vt)\frac{\omega}{v}\right]\right. \\ \left.-\mathrm{Im}[\zeta(T,d,K,\omega)]\sin\left[(y-vt)\frac{\omega}{v}\right]\right\}.\end{aligned} \tag{17}$$

Applying the conservation relations of energy and momentum, the upper and lower limits of k are given by

TABLE I. Values of parameters in Eq. (21) for Cu and Si.

Cu $\epsilon_b=1.05$			Si $\epsilon_b=1.06$		
$A_j(\mathrm{eV}^2)$	$\gamma_j(\mathrm{eV})$	$\omega_j(\mathrm{eV})$	$A_j(\mathrm{eV}^2)$	$\gamma_j(\mathrm{eV})$	$\omega_j(\mathrm{eV})$
64	0.01	0	8	0.12	3.42
20	0.1	0.3	15	0.35	3.52
6.5	0.65	2.5	45	0.66	3.80
5.5	0.7	3.1	82.8	0.5	4.25
4	0.7	3.7	5	2.42	4.55
55	2.6	5.05	32	1.1	5.34
42	4.76	8.93	52	3.4	6.4
172	10.18	14.74	15	5	9.4
80	8	25.6	15	6.5	14
240	32	40	6	5	18.4
100	30	55			
80	30	65			
412	37	85			

$$k_{\max}=\sqrt{2ME}+\sqrt{2ME-2M\omega}$$

and

$$k_{\min}=\sqrt{2ME}-\sqrt{2ME-2M\omega},$$

where M is the mass of the moving particle. Substituting the upper limit of integration in ω by $E=Mv^2/2$, we obtain

$$\begin{aligned}\phi_{\mathrm{ind}}^{(1)}(\mathbf{r},t)&=\frac{4q}{\pi^2}\int_0^E d\omega\int_{k_{\min}}^{k_{\max}}dk\int_{\omega/v}^{k}dK\frac{K\cos[(z-T/2)\sqrt{k^2-K^2}]}{k\sqrt{k^2-K^2}\sqrt{(vK)^2-\omega^2}}\\&\times\cos\left(x\frac{\sqrt{(vK)^2-\omega^2}}{v}\right)\left\{\mathrm{Re}[\zeta(T,d,K,\omega)]\right.\\&\left.\times\cos\left((y-vt)\frac{\omega}{v}\right)-\mathrm{Im}[\zeta(T,d,K,\omega)]\sin\left((y-vt)\frac{\omega}{v}\right)\right\}\end{aligned}\tag{18}$$

after changing the variable from θ to K according to $K=k\sin\theta$. Let ε_2 be the dielectric function of the substrate and $T=0$, we obtain the induced potential in vacuum for a semi-infinite solid. As Ritchie *et al.* have pointed out,[24] the present classical picture is applicable in the context of the first Born approximation quantum theory with the application of the energy-momentum conservation relations. This was explicitly explored in the derivation of the interaction between a moving charge and an electron gas.[25]

To compare with the corresponding expression by other authors without considering the energy-momentum conservation, no integration limits in momentum transfer are performed. Thus it is more convenient to carry out the integration in momentum of Eq. (13) using cylindrical coordinates instead of spherical coordinates. For a semi-infinite solid, i.e., $T=0$ and $\varepsilon_2=\varepsilon_3=\varepsilon$, we find

$$\begin{aligned}\phi_{\mathrm{ind}}^{(1)}(\mathbf{r},t)&=-\frac{q}{v\pi^2}\int_{-\infty}^{\infty}d\omega\int_{|\omega|/v}^{\infty}dK\frac{1}{\sqrt{K^2-(\omega/v)^2}}\\&\times\exp[-(|z|+d)K]\left[\frac{\varepsilon(K,\omega)-1}{\varepsilon(K,\omega)+1}\right]\\&\times\cos\left(\frac{\sqrt{(Kv)^2-\omega^2}}{v}x\right)\exp\left[i\frac{\omega}{v}(y-vt)\right].\end{aligned}\tag{19}$$

Taking $x=0$ and neglecting the spatial dispersion, we obtain the same results as those of Arista.[3]

Now, the stopping force is related to the derivative of $\phi_{\mathrm{ind}}^{(1)}(\mathbf{r},t)$ at the position of the particle $\mathbf{r}_0=(0,vt,D)$. For the case of an overlayer system, we obtain

$$\begin{aligned}-\frac{dW}{ds}&=-\frac{4q^2}{v\pi^2}\int_0^E d\omega\int_{k_{\min}}^{k_{\max}}dk\int_{w/v}^{k}dK\\&\times\omega\frac{K\cos[d\sqrt{k^2-K^2}]}{k\sqrt{k^2-K^2}\sqrt{(vK)^2-\omega^2}}\mathrm{Im}[\zeta(T,d,K,\omega)].\end{aligned}\tag{20}$$

The model response function used in this work is the extended Drude dielectric function.[15] This function may be expressed as

$$\varepsilon(\mathbf{k},\omega)=\varepsilon_b+\sum_j\frac{A_j}{\omega^2-(\omega_j+k^2/2)^2+i\omega\gamma_j},\tag{21}$$

where A_j, γ_j, and ω_j are, respectively, the oscillator strength, damping constant, and critical-point energy, all associated with the jth subband. The inclusion of a background dielectric constant, ε_b, is to account for the influence of polarized ion cores.[26] All these parameters are determined by a fit of the imaginary part of the dielectric function, $\mathrm{Im}[\varepsilon(0,\omega)]$, to experimental optical data. To assure the accuracy of the fitting parameters, we require that the fitted dielectric function satisfy the sum rules.

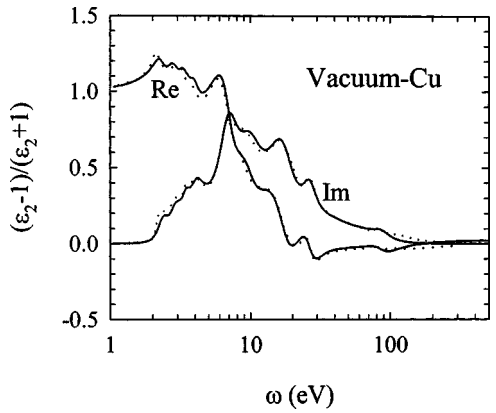

FIG. 2. A plot of the real and imaginary parts of the surface response function, in optical limit, vs energy transfer ω for a vacuum–Cu system. The solid curve is results calculated using the extended Drude dielectric functions with parameters listed in Table I. The dotted curve is deduced from measured optical data (Ref. 27).

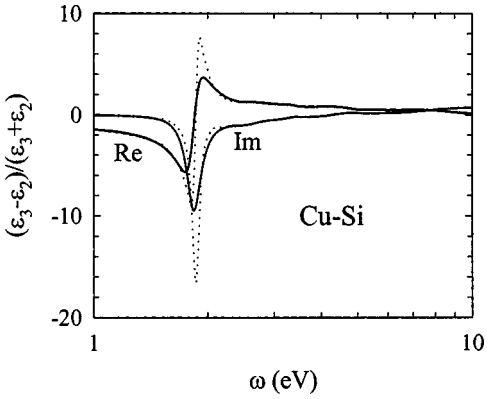

FIG. 3. A plot of the real and imaginary parts of the interface response function, in optical limit, vs energy transfer ω for a Cu–Si system. The solid curve is results calculated using the extended Drude dielectric functions with parameters listed in Table I. The dotted curve is deduced from measured optical data (Ref. 27).

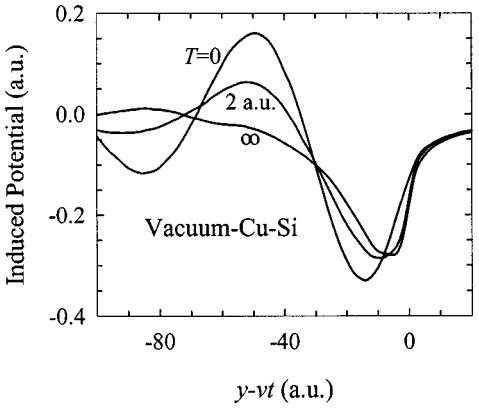

FIG. 5. The induced potential at points along the projection of the trajectory of the proton on the surface and at a distance $y-vt$ from the proton. Here we plot results for a vacuum–Cu–Si overlayer system with different Cu film thickness T. The proton is moving with velocity $v=5$ a.u. parallel to and at distance $d=1$ a.u. from the Cu surface. This potential indicates oscillations behind the position of the proton.

III. RESULTS AND DISCUSSION

We consider an overlayer system composed of a thin Cu film on a Si substrate. Parameters used in our calculations for the dielectric functions of Cu and Si are listed in Table I. Figure 2 shows the real and imaginary parts of the surface response function for a vacuum–Cu surface, i.e., $[\varepsilon_2(0,\omega)-1]/[\varepsilon_2(0,\omega)+1]$, versus energy transfer ω. Figure 3 shows a similar plot of the interface response function for a Cu–Si interface, i.e., $[\varepsilon_3(0,\omega)-\varepsilon_2(0,\omega)]/[\varepsilon_3(0,\omega)+\varepsilon_2(0,\omega)]$. Here $\varepsilon_2(0,\omega)$ and $\varepsilon_3(0,\omega)$ are dielectric functions of Cu and Si in the long-wavelength limit, i.e., $k\rightarrow 0$. In both figures, the solid curves are results calculated using the extended Drude dielectric functions. The dotted curves are corresponding results deduced from measured optical data.[27] It is seen that the present results and optical data are in good agreement, despite some deviation in magnitude at the peaks in Fig. 3. Our fitting strategy is that we require both the real and imaginary parts of the dielectric function to satisfy sum rules and to exhibit and match energy loss peaks for plasmon excitations and interband transitions. We also require that fitting results agree with optical data at a broad range of energy transfers. With this strategy, we are confident with the validity of fitting results regarding the energy losses in plasmon excitations and interband transitions. However, due to the limited optical data it is difficult to adjust fitting parameters to match fitting results to measured data at all energy transfers. The difference induced by this difficulty is magnified at peaks in the interface response function. However, such a difference makes little influence on the calculation of the induced potential and the stopping force studied in this work.

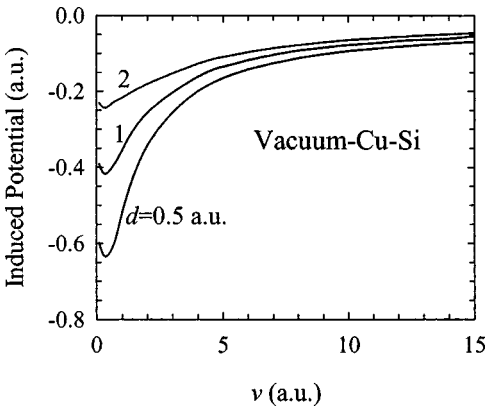

FIG. 4. Velocity dependence of the induced potential at the position of the proton moving parallel to a vacuum–Cu–Si overlayer system. The proton is at distance $d=0.5$, 1 and 2 a.u. from the surface of the Cu film (thickness $T=2$ a.u.).

Based on Eqs. (15) and (18) we have calculated the induced potential for a proton moving parallel to the surface of a vacuum–Cu–Si overlayer system. This potential at the position of the proton is plotted in Fig. 4 as a function of proton velocity for several proton distances, $d=0.5$, 1, and 2 a.u., from the Cu film of thickness $T=2$ a.u. Note that the magnitude of this potential decreases with increasing velocity and saturates at very large velocities. In all cases, there are dips around $v\leqslant 1$ a.u. As the distance of the proton from the Cu film becomes smaller the dip is deeper, a similar behavior observed for a slow proton moving parallel to the surface of a semi-infinite solid with plasmon-pole dielectric functions.[2] These dips occur at the threshold velocity for the creation of surface plasmons. For velocities smaller than the threshold velocity, only single electron–hole excitations occur. Our calculations of the induced potential at the position of a proton for a fixed distance from the Cu film of different thicknesses indicate that the dependence of this potential on film thickness is quite small.

Figure 5 illustrates the induced potential at points along the projection of the trajectory of a proton on the surface $(z=T/2)$ and at a distance $y-vt$ from the proton. Here we plot results for Cu films of thickness $T=0$, 2, and ∞ a.u. Note that y is the coordinate of the point along the projection of the proton on the surface. The proton is moving with velocity $v=5$ a.u. at a fixed distance, $d=1$ a.u., from the Cu surface. The instantaneous proton position is $y=vt$ and $z=1+T/2$. The induced potential reveals an oscillational behavior at points behind $(y<vt)$ the position of the proton.

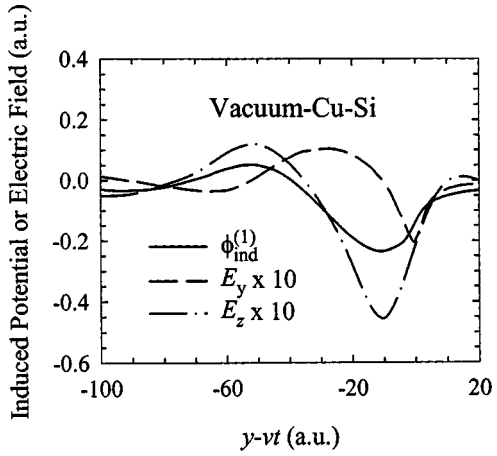

FIG. 6. The induced potential and electric field components at points along the trajectory of proton and at a distance $y-vt$ from the proton for a vacuum–Cu–Si overlayer system. The proton is moving with velocity $v=5$ a.u. parallel to and at distance $d=1$ a.u. from the surface of the Cu film of thickness $T=2$ a.u.

The influence of damping in the plasma modes on the induced potential is weak in the vacuum side. The gradual change in amplitude of this oscillation for different Cu films indicates a contribution from interface effects. Such a potential approaches that of a semi-infinite Si system ($T=0$) as Cu film thickness decreases. On the other hand, it approaches to that of a semi-infinite Cu system ($T=\infty$) as Cu film thickness increases. Figure 6 shows the induced potential, $\phi^{(1)}_{\mathrm{ind}}$, and the electric field components, E_y and E_z, at points along the particle trajectory ($z=d+T/2$) in front of ($y>vt$) and behind ($y<vt$) the proton. Here the proton is moving with velocity $v=5$ a.u. and at a distance $d=1$ a.u. from the Cu film of thickness $T=2$ a.u. It is seen that the induced potential has a shape of the wake potential. E_z and E_y oscillate, respectively, in phase and out of phase with the induced potential.

The dependence of the stopping force on proton velocity is illustrated in Fig. 7. Here we show the stopping force (solid curves) for a proton moving at a distance $d=2$ a.u. from the Cu films of thickness $T=0$, 1.5, and 4 a.u. The results of Arista (dotted curve) for a semi-infinite Cu system are included for comparison. Our results show a gradual change in the stopping force for varying thickness of Cu films. For $T=4$ a.u., the stopping force tends to approach that of a semi-infinite Cu system. In such a case, the lower values in the stopping force at small velocities found in this work are due to the constraints of energy-momentum conservation law. Notice that the maxima in Fig. 7 appear at a velocity around 1.5 a.u. and the stopping force drops to zero in the static limit. The existence of a maximum in the stopping force was also found by other theoretical models for a semi-infinite system.[3] The present work also reveals that the stopping force increases as proton distance decreases, a consequence due to the increased magnitude in the induced potential.

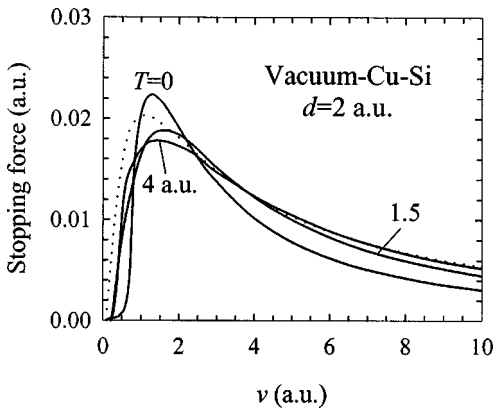

FIG. 7. Velocity dependence of the stopping force for a proton moving parallel to and at a distance $d=2$ a.u. from the surface of Cu films of different thicknesses in the vacuum–Cu–Si overlayer system. The solid curves are the results of present calculations. The dotted curve is the data of Arista (Ref. 3) for a semi-infinite Cu system.

IV. CONCLUSIONS

A dielectric response theory was used to describe the inelastic interactions between a charged particle and an overlayer system in the case of a parallel trajectory. In this theory, the response of the overlayer system was composed of surface and interface excitations and characterized in terms of dielectric functions of the film and the substrate. An extended Drude dielectric function was employed by the inclusion of the spatial dispersion effect. This function was built-up from measured optical data. The quantum effect of the moving particle was incorporated into the dielectric theory by considering the recoil effect. This effect was included by applying the conservation laws of energy and momentum. In this work, we have applied the continuum dielectric model to the overlayer system composed of a thin film and a substrate. The application of the model in the case of a thin film alone might be questionable. The validity of the model for an overlayer system was based on the continuum properties of the system and the inclusion of surface and interface charges and modifications.

Applying the method of image charges, analytical formulas have been derived for the calculation of the stopping force and the induced potential for charged particles moving parallel to the surface of an overlayer system. These formulas could be applied to any particles and overlayer systems. The approach could also be applied, in general, to any parallel trajectories inside and outside the solids. However, in the case of velocities smaller than the threshold of generating surface plasmons, only single particle–hole excitations contribute to the energy loss.[2,28] In such a case, it may be necessary to use the local-field-correction random-phase-approximation[29] instead of the Drude model to calculate dielectric functions.

An energetic charged particle moving parallel to the surface of an overlayer system was studied. Calculated results of the induced potential and the stopping force were presented for protons moving parallel to a vacuum–copper–silicon system. Corresponding experiments are, however, difficult due to the actual size and the bending of a beam. In such experiments, the beam size must be confined to a few angstroms. Otherwise, the surface and interface effects will

be averaging out and diminish. Because the induced potential or the stopping force decreases as particle velocity increases, as can be seen in Figs. 4 and 7, a fast particle is better than a slow particle for experimental measurements.

ACKNOWLEDGMENT

This research was sponsored by the National Science Council of the Republic of China under Contract No. NSC 90-2218-E-009-042.

[1] F. J. García de Abajo and P. M. Echenique, Phys. Rev. B **46**, 2663 (1992).
[2] F. J. García de Abajo and P. M. Echenique, Phys. Rev. B **48**, 13399 (1993).
[3] N. R. Arista, Phys. Rev. A **49**, 1885 (1994).
[4] R. H. Ritchie, Phys. Rev. **106**, 874 (1957).
[5] R. H. Ritchie and A. L. Marusak, Surf. Sci. **4**, 234 (1966).
[6] F. Bloch, Z. Phys. **81**, 363 (1933).
[7] B. I. Lundqvist, Phys. Status Solidi **32**, 273 (1969).
[8] J. Lindhard, K. Dan. Vidensk. Selsk. Mat. Fys. Medd. **28**, 1 (1954).
[9] J. Burgdörfer, Nucl. Instrum. Methods Phys. Res. B **67**, 1 (1992).
[10] P. Focke, S. Suárez, R. Pregliasco, and W. Mekbach, Nucl. Instrum. Methods Phys. Res. B **67**, 1 (1992).
[11] T. Iitaka, Y. H. Ohtsuki, A. Koyama, and H. Ishikawa, Phys. Rev. Lett. **65**, 3160 (1990).
[12] K. Kimura, M. Tsuji, and M. Mannami, Phys. Rev. A **46**, 2618 (1992).
[13] P. E. Batson, Ultramicroscopy **11**, 299 (1983).
[14] A. Howie and R. H. Milne, Ultramicroscopy **18**, 427 (1985).
[15] C. M. Kwei, Y. F. Chen, C. J. Tung, and J. P. Wang, Surf. Sci. **293**, 202 (1993).
[16] C. J. Tung, Y. F. Chen, C. M. Kwei, and T. L. Chou, Phys. Rev. B **49**, 16684 (1994).
[17] Y. F. Chen, P. Su, C. M. Kwei, and C. J. Tung, Phys. Rev. B **50**, 17547 (1994).
[18] Y. F. Chen, C. M. Kwei, and P. Su, J. Phys. D **28**, 2163 (1995).
[19] C. M. Kwei, P. Su, Y. F. Chen, and C. J. Tung, J. Phys. D **30**, 13 (1997).
[20] C. M. Kwei, S. Y. Chiou, and Y. C. Li, J. Appl. Phys. **85**, 8247 (1999).
[21] C. M. Kwei, S. S. Tsai, and C. J. Tung, Surf. Sci. **473**, 50 (2001).
[22] F. Yubero and S. Tougaard, Phys. Rev. B **46**, 2486 (1992).
[23] F. Yubero, J. M. Sanz, B. Ramskov, and S. Tougaard, Phys. Rev. B **53**, 9719 (1996).
[24] R. H. Ritchie *et al.*, in *Physical and Chemical Mechanisms in Molecular Radiation Biology*, edited by W. A. Glass and N. V. Varma (Plenum, New York, 1991), p. 99.
[25] F. Flores, in *Interaction of Charged Particles with Solids and Surfaces*, edited by A. Gras-Marti, H. M. Urbassek, N. R. Arista, and F. Flores (Plenum, New York, 1991), p. 3.
[26] D. Y. Smith and E. Shiles, Phys. Rev. B **17**, 4689 (1978).
[27] E. D. Palik, *Handbook of Optical Constants of Solids I* (Academic, New York, 1985).
[28] C. M. Kwei, J. J. Chou, J. Yao, and C. J. Tung, Phys. Rev. A **64**, 042901 (2001).
[29] K. Utsumi and S. Ichimaru, Phys. Rev. A **26**, 603 (1982).